Received: 3 June 2026 | Revised: 15 July 2026 | Accepted: 22 July 2026

DOI: 10.1002/pro.70738

RESEARCH ARTICLE

THE PROTEIN SOCIETY WILEY

Engineered antibodies preserve structural and functional recognition of *Plasmodium falciparum* circumsporozoite protein

Monika Jain[1] | **Sashank Agrawal**[1] | **Fabien Cannac**[1] | **Gonzalo E. González-Páez**[1] | **Wen-Hsin Lee**[1] | **Re'em Moskovitz**[1] | **Randal R. Ketchem**[2] | **Katherine L. Williams**[3] | **Daniel E. Emerling**[3] | **Andrew B. Ward**[1] | **Ian A. Wilson**[1,4]

[1]Department of Integrative Structural and Computational Biology, The Scripps Research Institute, La Jolla, California, USA

[2]Just-Evotec Biologics, Seattle, Washington, USA

[3]Atreca, Inc., San Carlos, California, USA

[4]The Skaggs Institute for Chemical Biology, The Scripps Research Institute, La Jolla, California, USA

Correspondence
Ian A. Wilson, Department of Integrative Structural and Computational Biology, The Scripps Research Institute, La Jolla, CA 92037, USA.
Email: wilson@scripps.edu

Present addresses
Randal R. Ketchem, Ketchem Biotherapeutics Consulting LLC, USA; Katherine L. Williams, Gilead Sciences, USA; and Daniel E. Emerling, Annexon Biosciences, USA.

Funding information
Gates Foundation, Grant/Award Numbers: INV-004923, INV-056202

Review Editor: Jeanine F. Amacher

Abstract

Long-lasting and highly effective malaria vaccines or monoclonal antibodies (mAbs) remain urgently needed, as current interventions show age-dependent benefits rather than broad protection across all ages. Recently, two highly protective human mAbs 224 (IGHV3-49/IGLV1-40) and 7088 (IGHV3-33/IGKV1-5), encoded by distinct germline genes, were re-engineered and renamed MAM01 and MS-1805, respectively, to extend serum half-life and enable low-cost, large-scale manufacturing in alignment with WHO guidelines. MAM01 completed Phase I and IIb clinical trials (safety/PK/challenge) in US healthy naive adults and is now in Phase I trials (age-de-escalation studies) in Uganda. Here, we determined crystal structures of the antigen-binding fragments (Fabs) of engineered MAM01, MS-1805, and 7088 in complex with different regions of the *Plasmodium falciparum* circumsporozoite protein (PfCSP), including junctional, minor, and major repeat regions. Notably, Fab 7088 features an extended CDRL3 comprising 10 amino acids (CDRL3:10) instead of the canonical 8 amino acid CDRL3 (CDRL3:8) typically observed in V_H3-33/V_K1-5-encoded mAbs, indicating unique folding within its germline context. In addition, cryo-EM structures of Fabs 7088 and MS-1805, in complex with recombinant shortened CSP (rsCSP), revealed a regular spiral configuration stabilized by homotypic Fab-Fab interactions, whereas 224 and MAM01 did not form such assemblies. Structural comparisons demonstrated that engineered antibodies retained key molecular and hydrogen-bond interactions without significant conformational changes, thereby maintaining antigen recognition and preserving binding affinity. These findings demonstrate that targeted framework engineering can enhance therapeutic potential while preserving structural integrity and function, providing insights for next-generation antibody-based interventions against malaria.

KEYWORDS
cryo-EM, crystal structures, engineered human mAbs, epitopes, malaria, MAM01, PfCSP

1 | INTRODUCTION

Malaria is still a major global concern and public health threat due to emerging environmental factors associated with climate change and vector resistance to insecticides (Suh et al., 2023; Thomson & Stanberry, 2022). In 2024, 282 million cases of malaria were reported worldwide, and infection with *Plasmodium falciparum*, the deadliest species of the malaria parasite, led to high mortality among young children and pregnant women, particularly in sub-Saharan Africa and Southeast Asia (World Malaria Report, 2025).

Despite recent advances and approved vaccines, including RTS,S/AS01 (Mosquirix) and R21/Matrix-M, protection remains incomplete and short-lived, underscoring the need for improved interventions targeting conserved parasite vulnerabilities (Datoo et al., 2024; Zavala, 2022). However, several highly protective human monoclonal antibodies (mAb) have been isolated from participants vaccinated with RTS,S/AS01, including mAbs 317 and 311 (Oyen et al., 2017) or immunized with an attenuated whole sporozoite vaccine (PfSPZ vaccine), including mAb L9 and CIS43 (Kayentao et al., 2022; Wu et al., 2022). Treatment with these mAbs, which target different regions of the CSP, inhibits sporozoite infection and demonstrates protection from malaria in mouse models (Flores-Garcia et al., 2021; Livingstone et al., 2021; Wang et al., 2020). Recent clinical trials have shown that human L9 and CIS43 mAbs, which target the CSP minor region and junctional region, respectively, prevent infection against malaria (Gaudinski et al., 2021; Kayentao et al., 2024; Nekkab & Penny, 2022). Both antibodies were further optimized by introducing LS point mutations (M428L/N434S) in the fragment crystallizable (Fc) region C_H3 domain to extend their half-life and were named L9LS and CIS43LS (Kayentao et al., 2024; Kisalu, et al., 2021).

More recently, two highly potent anti-CSP antibodies 224 and 7088 were isolated from protected individuals administered with the RTS,S/AS01, and engineered and renamed MAM01 and MS-1805, respectively, to improve stability, half-life, and manufacturability (Williams et al., 2024). Antibodies 224 and 7088 were subsequently engineered by introducing specific mutations in the framework regions of their variable domains, along with LS mutations in the Fc region, to enhance their stability and extend half-life for use as therapeutics (Ducancel & Muller, 2012; Zalevsky et al., 2010). The engineered 224, renamed MS-1797 (MAM01), was selected as the main drug candidate and advanced into clinical development, whereas the engineered 7088, renamed MS-1805, was designated as a backup candidate for malaria prevention (Miura et al., 2024; Williams et al., 2024). However, whether such engineering alters antigen recognition or the structural basis of PfCSP engagement remains unclear. Here, we test the hypothesis that the developability-focused framework and Fc engineering do not perturb Fab conformation, CDR architecture, or PfCSP binding mode. Thus, we determined x-ray crystal structures of the engineered Fabs in complex with PfCSP peptides, together with cryo-electron microscopy structures of Fab-PfCSP assemblies.

MAM01 and MS-1805 retained their binding to peptides derived from different CSP regions, albeit with slightly lower binding affinities compared to the antibodies 224 and 7088. Structural characterization of the Fabs of engineered antibodies MAM01 and MS-1805 revealed no significant conformational changes in the overall antibody structure, their complementarity-determining regions (CDRs), hydrogen bond interactions, or homotypic states compared to 224 and 7088. These findings demonstrate that targeted modifications can be introduced into naturally occurring antibodies without disrupting their structural integrity, while improving stability and large-scale manufacturability.

We further observed that 7088 Fab possesses an extended CDRL3 of 10 amino acids (CDRL3:10), which differs from the typical CDRL3 of 8 amino acids (CDRL3:8) observed in other CSP repeat antibodies encoded by the IGHV3-33 and IGKV1-5 germline genes (Imkeller et al., 2018; Thai et al., 2023). From the crystal structures of Fabs 7088 and MS-1805, we were able to understand how the long CDRL3 of 10 amino acids is accommodated in the context of the IGHV3-33/IGKV1-5 germline-encoded antibody. Furthermore, the cryo-EM structures of 7088 and MS-1805 with rsCSP revealed the formation of well-ordered spiral conformations stabilized by homotypic Fab-Fab interactions, whereas such spiral assemblies are not observed for 224 and MAM01 with rsCSP. Together, our findings demonstrate that targeted engineering of anti-CSP antibodies can enhance developability without compromising structural integrity or antigen recognition. These results provide a structural framework for the rational design of next-generation monoclonal antibodies for malaria prevention.

2 | RESULTS

2.1 | Binding affinity of Fabs 224 and 7088 and engineered Fabs MAM01 and MS-1805 to PfCSP-derived epitopes of different regions

The antibody sequences of 224 and 7088 were identified from plasmablasts isolated from protected participants enrolled in a Phase IIa clinical trial of RTS,S/AS01 (Regules et al., 2016). For clinical trials, these mAbs were engineered by mutating specific residues and renamed MAM01 and MS-1805, respectively,

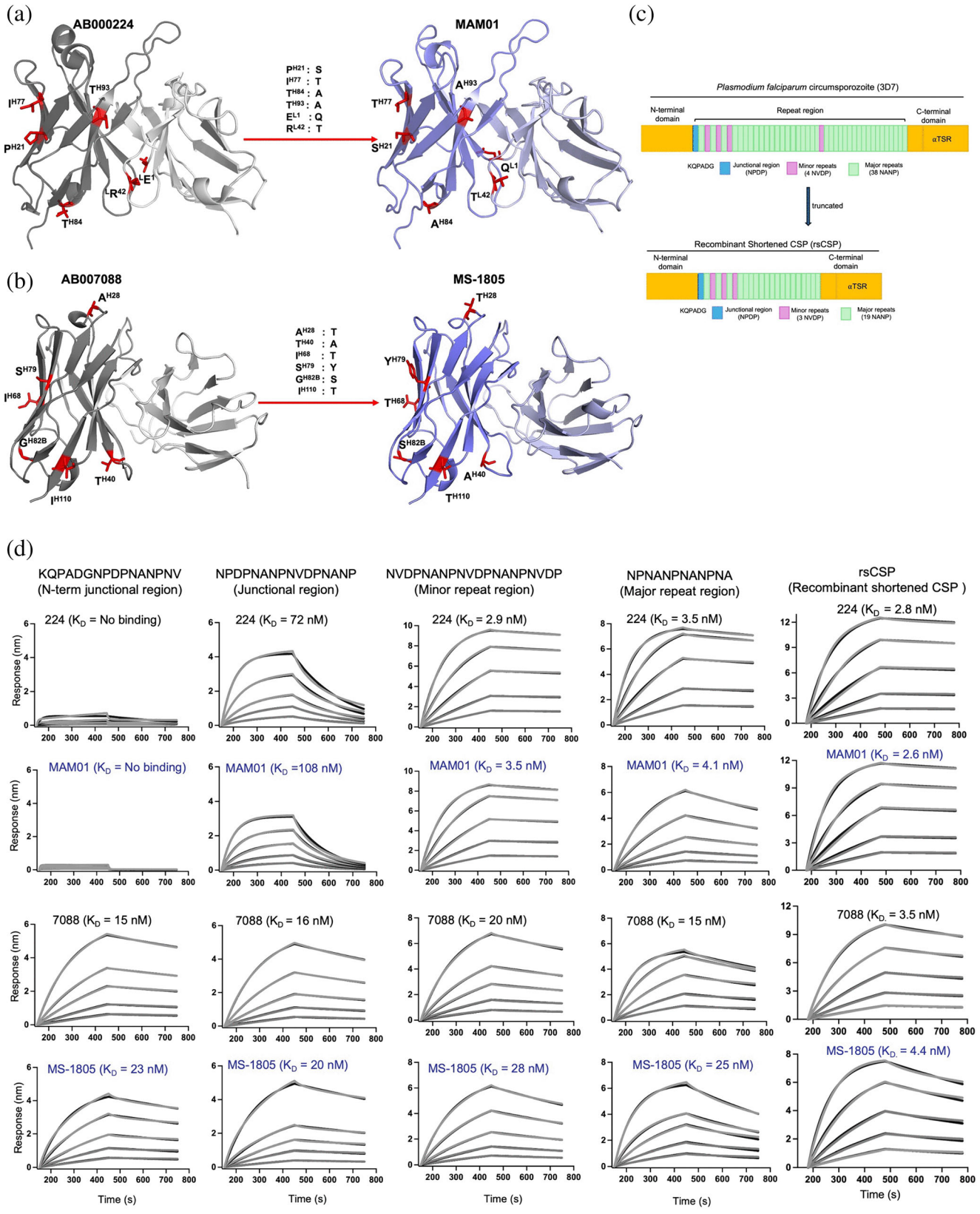

FIGURE 1 Legend on next page.

which enhanced their stability, half-life, and manufacturability at lower cost (Williams et al., 2024). For MAM01, mutations were introduced in the variable domain framework region of the heavy chain of the 224 antibody. Proline, isoleucine, and threonine residues were replaced with serine at amino acid position 21, threonine at position 77, and alanine at positions 84 and 93 (Kabat numbering) (Figure 1a). Additionally, in the Fv region of the light chain, glutamic acid and arginine residues were replaced with glutamine at position 1 and threonine at position 42, respectively (Figure 1a). In contrast, modifications in engineered 7088 were restricted to the heavy chain with no changes in the light chain. For MS-1805, specific mutations included replacing alanine at position 28 and isoleucine at position 68 and 110 with threonine, while glycine at 82B, serine at position 79, and threonine at position 40 were replaced with serine, tyrosine, and alanine, respectively (Figure 1b). Outlier amino acid residues in the framework regions were substituted with mutations previously reported to enhance molecular stability, which in turn improves overall developability (Kerwin et al., 2020; Williams et al., 2024). For both antibodies, LS mutations at (M428L/N434S) were introduced in the Fc region to extend half-life, but the effect of these mutations is not analyzed here, as we are focusing on the Fabs of these antibodies.

We analyzed and compared the binding affinity of Fabs 224 and 7088 with the engineered Fab MAM01 and MS-1805 for CSP-derived peptides from different regions, including the N-terminal junctional region (KQPADGNPDPNANPNV), junctional region (NPDPN ANPNVDPNANP), minor repeat region (NVDPNA NPNVDPNANPNVDP), and major repeat region ($NPNA_3$) (Figure 1c). Bio-layer interferometry (BLI) was performed to analyze the binding affinity and kinetics of these Fabs to the CSP-derived peptides (Table S1). We observed that Fab MAM01 binds with high affinity (K_D 3–4 nM) to the minor and major repeat regions compared to the junctional region (K_D 108 nM), retaining comparable affinity to these peptides as Fab 224 (Figure 1d). However, Fab MS-1805 binds to all of these peptides with high affinity (K_D 20–28 nM), which were comparable to Fab 7088 (K_D 15–20 nM). Notably, we found that Fab 7088 and MS-1805 also bind to peptides from the N-terminal junctional region (KQPADG), while Fab 224 and MAM01 showed no binding to this region. These results suggest that the N-terminus of the CSP junctional region of PfCSP might be involved in binding to Fabs 7088 and MS-1805 (Figure 1d).

We further evaluated binding in a more native-like context by measuring affinities to recombinant shortened CSP (rsCSP). Fab MAM01 and Fab 224 exhibited slightly higher K_D values of 2.6 and 2.8 nM, respectively, while Fab 7088 and MS-1805 showed improved binding to rsCSP compared to their isolated peptides (K_D 3.5–4.4 nM). This enhanced affinity to rsCSP likely reflects avidity effects arising from multivalent epitope presentation (Figure 1d, Table S1).

2.2 | Crystal structures of engineered MAM01 Fab with CSP-derived peptides of junctional, minor repeat, short major repeat, and long major repeat regions

Crystal structures of MAM01 Fab in complex with CSP-derived peptides from the junctional region, minor repeat region, short major repeat region ($NPNA_3$), and long major repeat region ($NANP_6$) were determined to elucidate the structural basis of MAM01 binding to various CSP-derived peptides (Figure 2a). The crystals diffracted to 2.71, 1.84, 1.54, and 1.48 Å resolution, respectively (Table S2).

The interactions between Fab MAM01 and the peptides are mediated through heavy chain CDRH2 and CDRH3, and light chain CDRL1 and CDRL3. In the MAM01 Fab complex with junctional peptide (^{1}NPDPNA NPNVDPNA^{14}), residues were assigned numbers from 1 to 14, although the electron density was not well defined for Asn^{1} (Figure 2b). Similarly, for minor repeat peptide (^{1}NVDPNANPNVDPNANPNVDP^{20}), residues were numbered from 1 to 20, but no electron density was visible for Asn^{1} to Asn^{5} (Figure 2c). In the MAM01 complex with short major repeat (^{1}NPNANPNANPNA^{12}), residues were numbered from 1 to 12 with well-defined electron density for all residues (Figure 2d). For the long major repeat (^{1}NANPNANPNANPNANPNANPNANP^{24}), residues were numbered from 1 to 24, although no

FIGURE 1 Binding kinetics for Fabs with PfCSP-derived epitopes from different regions analyzed in this study. (a), (b) Cartoon representation of the polypeptide backbone of the heavy and light variable chains for Fabs 224 and 7088 and engineered Fabs MAM01and MS-1805. For 224 and 7088 Fabs, the heavy chain is shown in dark gray and the light chain in light gray, while for engineered Fabs, the heavy chain is in dark blue and the light chain in light blue. Mutations introduced primarily in the framework regions of Fabs 224 and 7088 to generate MAM01 and MS-1805, respectively, are marked in red, and the residues labeled with their locations in superscript (Kabat numbering). (c) Schematic representation of the domain organization of PfCSP, along with the truncated version rsCSP used for binding and structural studies. (d) Bio-layer interferometry analysis of binding kinetics for both 224 and 7088 and their engineered Fabs with various PfCSP-derived peptides and rsCSP. Representative sensorgrams (gray) and corresponding fits using a 1:1 global binding model (black) are shown. Serial dilutions of Fab concentrations (200, 100, 50, 25, and 12.5 nM) are presented from top to bottom. Equilibrium dissociation constants (K_D) for each Fab-peptide interaction are indicated (see also Table S1).

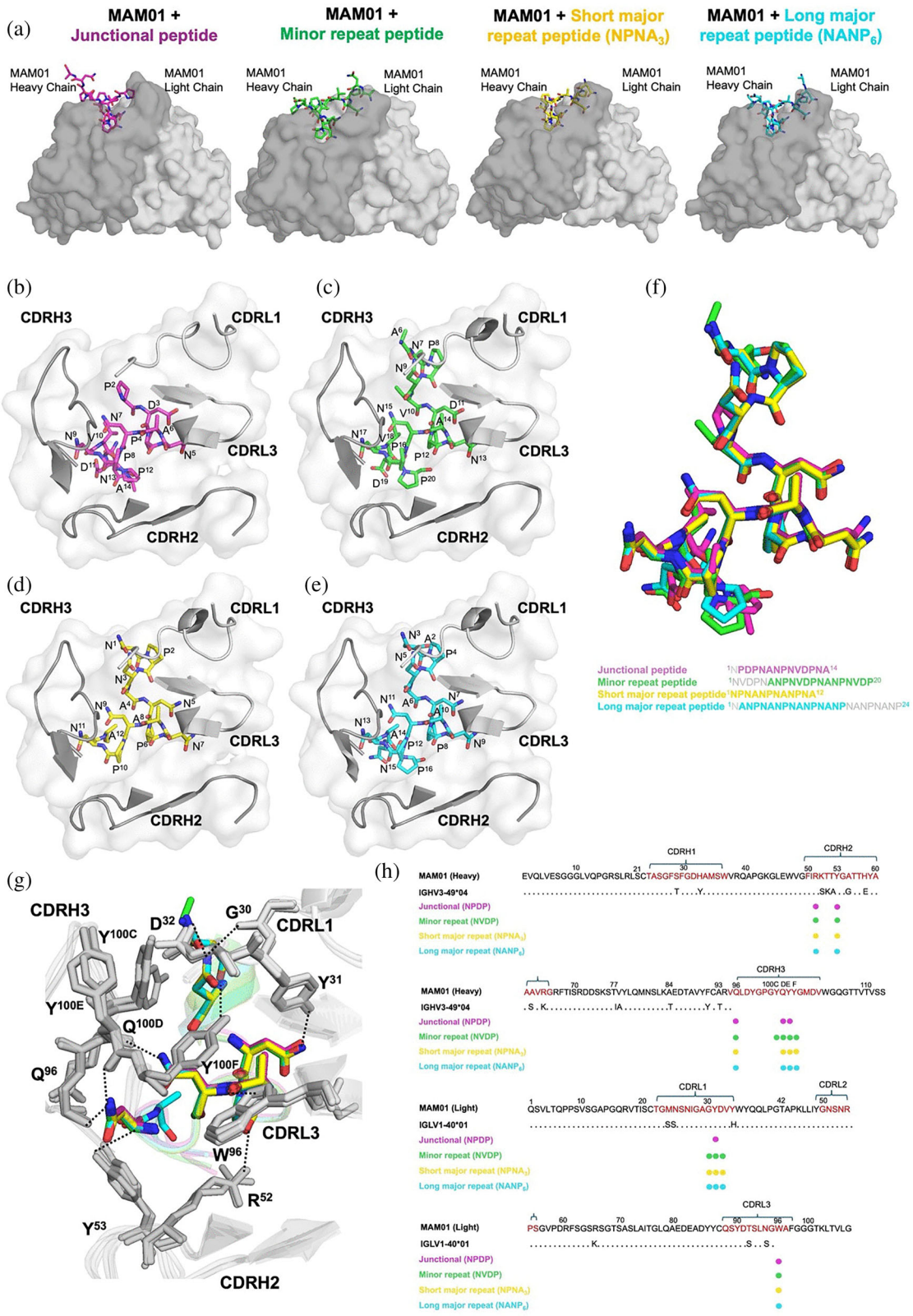

FIGURE 2 Crystal structures of MAM01 Fab with CSP-derived peptides. (a) Surface representation of MAM01 Fab bound to peptides from junctional (magenta), minor repeat (green), short major repeat (yellow), and long major repeat (cyan) regions. Variable domains are colored dark gray for heavy chain and light gray for light chain. (b)–(e) Close-up view of MAM01 CDRs interacting with each peptide: (b) junctional (magenta), (c) minor repeat (green), (d) short major repeat (yellow), and (e) long major repeat (cyan). (f) Superimposed peptides are colored according to sequence. (g) Hydrogen-bond interactions between MAM01 and peptides are highlighted in black dashes. (h) MAM01 Fab sequence (Kabat numbering) with CDR residues interacting with each peptide marked as closed circles (colored by peptide region).

electron density was visible for Asn^{17} to Pro^{24} and was not well defined for Asn^{1} (Figure 2e). The experimental electron density for all of these peptides bound to MAM01 Fab is shown in (Figure S1A). MAM01 bound to all CSP-derived peptides in a similar manner, and their superimposition revealed that all of the peptides adopted secondary structural motifs corresponding to type I β-turn conformations with high similarity in the central type I β-turn (Figures 2f, S1B,C). The core of the major repeat region displayed an identical conformation to the core of the minor repeat region, with all epitopes forming similar hydrogen bond interactions with heavy chain $^{H}Arg^{52}$, $^{H}Tyr^{53}$, $^{H}Gln^{96}$, $^{H}Gln^{100D}$, and $^{H}Tyr^{100E}$, and light chain $^{L}Gly^{30}$, $^{L}Tyr^{31}$, $^{L}Asp^{32}$, and $^{L}Trp^{96}$ in the MAM01 paratope (Figure 2g). However, fewer hydrogen-bond interactions were observed for the MAM01 Fab complexed with the junctional region peptide in CDRL1 and CDRH3 (Figure 2h).

Furthermore, we compared the crystal structure of Fab MAM01 with the short major repeat region peptide ($NPNA_3$) with our previously determined antibody Fab 224 complex with $NPNA_3$ (PDB ID: 6WFY) (Pholcharee et al., 2021) to investigate whether any structural conformational changes were observed after the antibody modifications (Figure 3a,b). MAM01 Fab with short major repeat region peptide ($NPNA_3$) crystallized in a $P2_12_12_1$ space group, whereas Fab 224 in complex with $NPNA_3$ crystallized in a $P2_1$ space group, each with a single complex in the crystal asymmetric unit (asu). Alignment of Fab MAM01 and Fab 224 complexes with $NPNA_3$ yielded a low RMSD of 0.15 Å for all C-alpha atoms in the Fab variable domains (Figure 3c).

The short major repeat peptide $NPNA_3$ binds to Fab 224 and MAM01 in a similar type I β-turn conformation (Figure S1C). The interactions with CDR loops and the hydrogen-bond patterns are all conserved in the 224 and engineered MAM01 Fabs. The buried surface area (BSA) for the Fab MAM01-$NPNA_3$ complex is primarily contributed by the heavy chain (446 $Å^2$ on the Fab and 496 $Å^2$ on the peptide), similar to Fab 224-$NPNA_3$ complex (443$Å^2$ on the Fab and 496 $Å^2$ on the peptide). Light-chain contributions of MAM01 are mediated by CDRL1 and CDRL3 (BSA: 252 $Å^2$ on the Fab and 264 $Å^2$ on the peptide), comparable to those in the Fab 224-$NPNA_3$ complex (BSA: 256 $Å^2$ on the Fab and 263 $Å^2$ on the peptide) (Figure 3d). The highest contributions to the BSA come from P^{10}, N^{11}, N^{3}, N^{7} in $^{3}NANPNANPNA^{12}$ in both crystal structures (Figure S2).

Furthermore, the MAM01-peptide complexes have similar Trp-Pro interactions and Trp-hydrogen bonds as Fab 224 with the $NPNA_3$ peptide. Fab 224 and MAM01 both engage in CH/π interactions with germline-encoded $^{H}Phe^{50}$ in CDRH2 and similar hydrogen bond interactions between conserved $^{L}Trp^{96}$ in CDRL3 and the alanine backbone (Figure 3e).

2.3 | Crystal structures of mAb 7088 Fab and MS-1805 Fab with junctional and short major repeat regions

Although mAb 7088, was engineered to MS-1805 as an alternative candidate for malaria prevention, structural data for 7088 Fab, both alone and in complex with CSP-derived peptides, were previously unavailable. Here, we determined crystal structures of Fab 7088 and its engineered counterpart MS-1805, with peptides derived from the short major repeat ($NPNA_3$) and N-terminal junctional region. Crystals of Fab 7088 diffracted to 3.20 and 2.0 Å resolution for the N-terminal junctional and short major repeat regions, respectively (Figure 4a and Table S3), and crystals of Fab MS-1805 diffracted to 1.74 Å for the N-terminal junctional region and 2.25 Å for the short major repeat region (Figure 4b and Table S3).

In Fab 7088 and Fab MS-1805 with $NPNA_3$, electron density was not observed for the initial three residues (Asn^{1} to Asn^{3}). Similarly, for Fab 7088 and MS-1805 with the N-terminal junctional peptide ($^{1}KQPADGNPDPNANPNV^{16}$), no electron density was present for the initial six residues (Lys^{1} to Gly^{6}) (Figures 4c,d, and S3A), indicating that the KQPADG region is disordered and not essential for binding. The Fab 7088 with the short major repeat region ($NPNA_3$) crystallized in a $P4_32_12$ space group, while Fab 7088 with the N-terminal junctional region crystallized in space group $P2_12_12_1$ with a single complex in the crystal asymmetric unit. The engineered Fab MS-1805 with $NPNA_3$ and also the N-terminal junctional region crystallized in a $P2_1$ space group with a single complex in the crystal asymmetric unit. Interactions between Fab 7088 and engineered Fab MS-1805 with their CSP-derived peptides are mainly mediated through CDRH1, H2, and H3, and CDRL3. Both Fab 7088 and its engineered counterpart Fab MS-1805 bound their peptides in a similar Asn pseudo 3_{10}-turn and type I β-turn conformation (Figures 4e and S3B).

Fab 7088 and MS-1805 complexes with the major repeat region peptide showed an almost identical conformation to those complexed with the N-terminal junctional region, with all epitopes forming similar hydrogen-bond interactions. Key conserved interactions are made with heavy chain $^{H}Thr^{31}$, $^{H}Gly^{33}$, $^{H}Tyr^{52A}$, $^{H}Ser^{98}$, $^{H}Gly^{100}$, $^{H}Pro^{100A}$, $^{H}Gly^{100C}$, and light chain $^{L}Asn^{92}$, $^{L}Tyr^{94}$, $^{L}Ser^{95}$, and $^{L}Phe^{95A}$ in the paratope of Fab 7088 and MS-1805 (Figure 4f).

We further superimposed the crystal structure of Fab MS-1805 with Fab 7088 in complex with both short major repeat ($NPNA_3$) and N-terminal junctional region peptides to investigate potential differences in epitope interactions or conformation. The epitope interactions with CDR loops were similar, with conserved hydrogen-bond interactions in both 7088 and MS-1805 Fabs with $NPNA_3$ (Figure 5a). The buried surface area (BSA) for

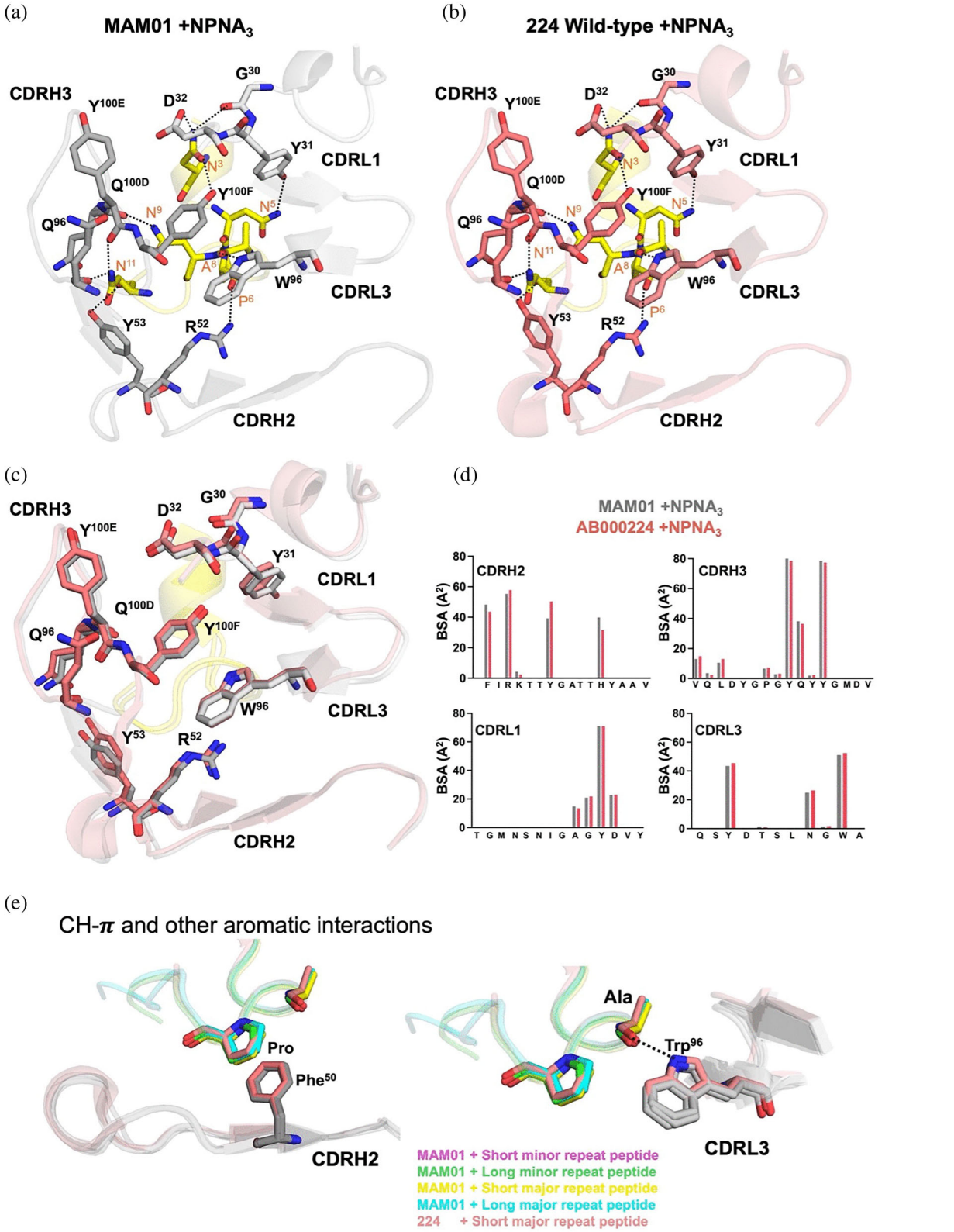

FIGURE 3 Conserved interactions of 224 and MAM01 Fabs. (a) Crystal structure of MAM01 with $NPNA_3$. (b) Crystal structure of Fab 224 with $NPNA_3$ (PDB ID: 6WFY). Only CDRs involved in peptide interactions are shown. Residues forming hydrogen bonds are shown as sticks. (c) Structural alignment of Fabs 224 (salmon) and MAM01 (gray) with $NPNA_3$ (yellow). (d) Bar plot showing buried surface area contributions of CDRs H2, H3, L1, and L3 in Fab 224 (salmon) and MAM01 (gray). (e) Superimposed view of aromatic residues in Fabs 224 (PDB ID: 6WFY) and MAM01 interacting with CSP-derived peptides from different regions.

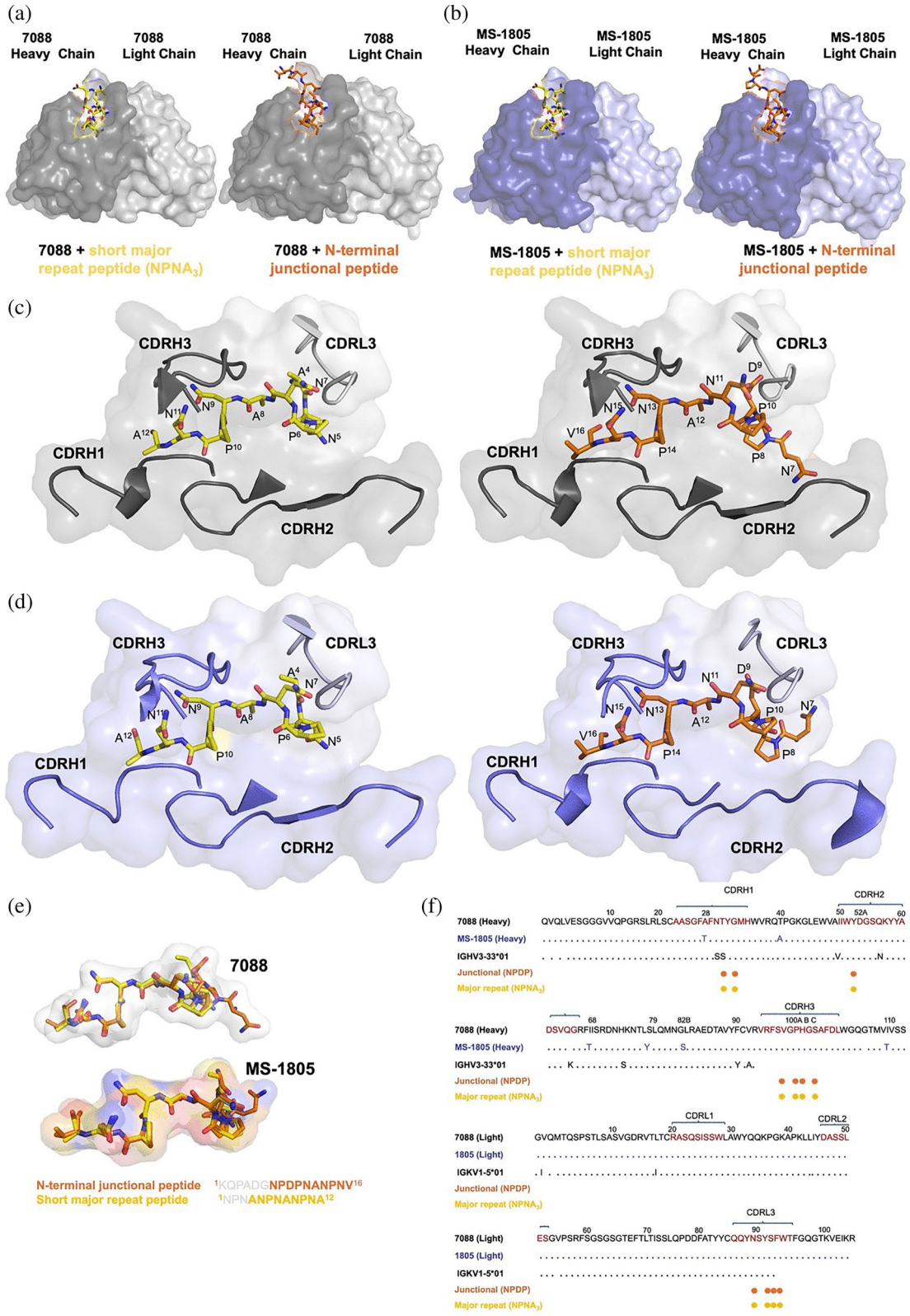

FIGURE 4 Crystal structures of Fab 7088 and MS-1805 with CSP-derived peptides. (a) Surface representation of Fab 7088 (heavy chain: gray, light chain: white) with short major repeat (yellow sticks) and junctional (orange sticks) peptides. (b) Structure of engineered Fab MS-1805 (heavy chain: dark blue, light chain: light blue) with the same peptides. (c), (d) CDRs involved in interactions with peptides in Fab 7088 (gray) and MS-1805 (blue), are shown as cartoons. (e) Superimposition of N-terminal junctional and major repeat peptides of 7088 and MS-1805 embedded in transparent surface rendering is represented as sticks and colored with respect to the sequences observed in the electron density. (f) Sequence of Fabs 7088 (black) and MS-1805 (blue) with CDR residues interacting with each peptide marked as closed circles, color-coded by peptide region.

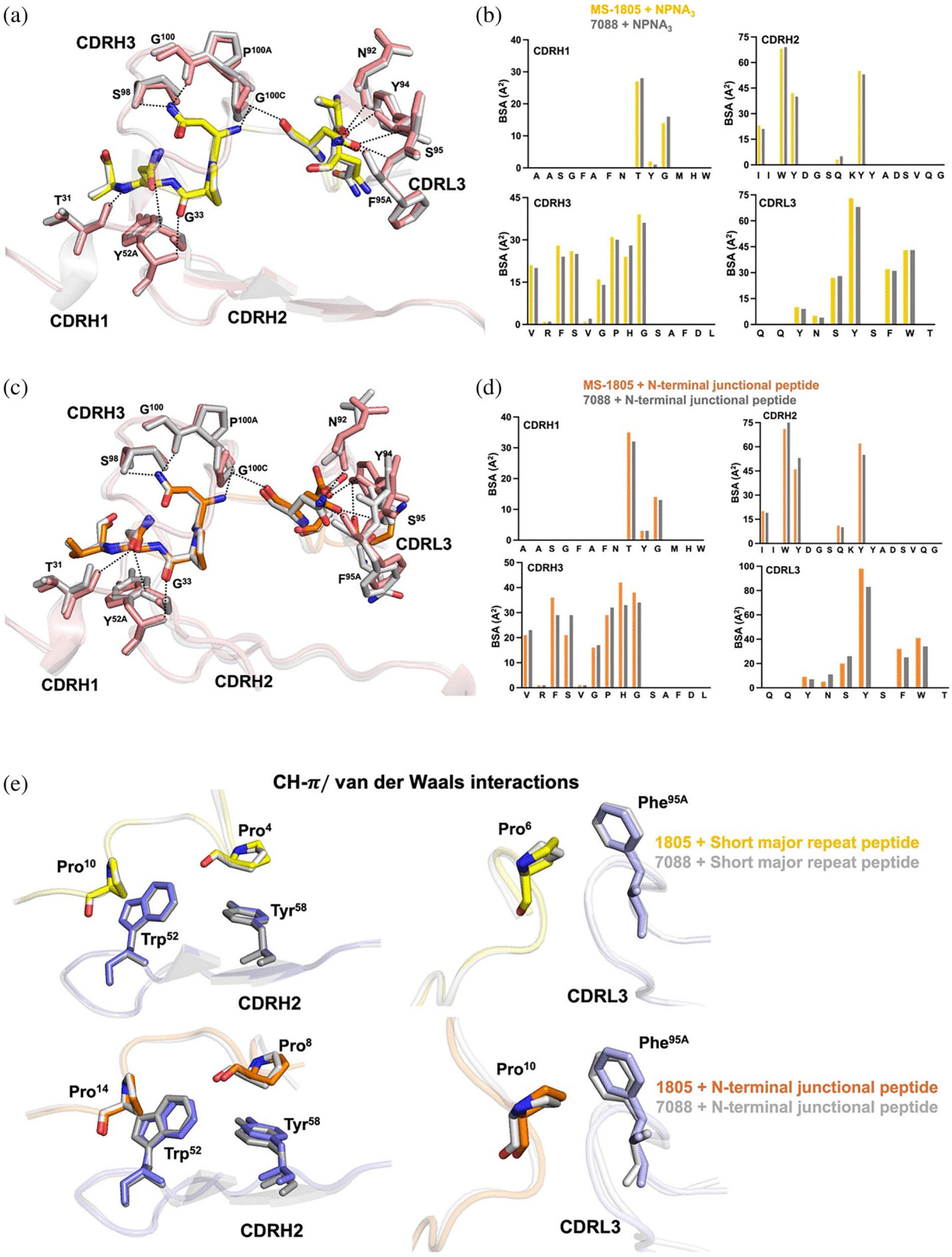

FIGURE 5 Conserved hydrogen bonding in Fabs 7088 and MS-1805. (a) Structural alignment of Fabs 7088 (gray) and MS-1805 (salmon) with $NPNA_3$. CDR residues involved in hydrogen bonds are shown as sticks. (b) Bar plot of buried surface area contributions of CDRs H1, H2, H3, and L3 in Fab 7088 (gray) and MS-1805 (yellow). (c) Structural alignment of Fab 7088 and MS-1805 with the N-terminal junctional peptide (orange). (d) Bar plot showing buried surface area contributions of CDRs H1, H2, H3, and L3 for Fabs 7088 (gray) and MS-1805 (orange). (e) Superimposed aromatic residues in Fabs 7088 (gray) and MS-1805 (blue) with CSP-derived peptides.

Fab MS-1805-$NPNA_3$ complex is predominantly contributed by heavy chain (443 $Å^2$ on the Fab and 560 $Å^2$ on the peptide), as in the Fab 7088-$NPNA_3$ complex (421$Å^2$ on the Fab and 526 $Å^2$ on the peptide). Contributions from the light chain are mediated exclusively by CDRL3 (189 $Å^2$ on the Fab and 248 $Å^2$ on the peptide), like those in the Fab 7088-$NPNA_3$ complex (BSA is 182 $Å^2$ on the Fab and 234 $Å^2$ on the peptide) (Figure 5b).

Notably, we observed slight differences in the initial residues ^{7}NPD^{9} of the N-terminal junctional epitope in the MS-1805 complex, which interacts with CDRH3, compared to the Fab 7088 complexed with the same peptide. This minor difference may be due to the lower resolution of the Fab 7088 structure and the less resolved density of the peptide and CDRH3 loop (Figure S3C). However, the epitope interactions and hydrogen bonds with CDRs were conserved in both 7088 and MS-1805 Fabs complexes with the N-terminal junctional peptide (Figure 5c). The BSA for the Fab MS-1805 with N-terminal junctional peptide complex is primarily contributed by the heavy chain (463 $Å^2$ on the Fab and 587 $Å^2$ on the peptide), similar to that for the Fab 7088 complex (446 $Å^2$ on the Fab and 582 $Å^2$ on the peptide). The light chain BSA is mediated solely by CDRL3 (208 $Å^2$ on Fab and 251 $Å^2$ on peptide), similar to Fab 7088 (198 $Å^2$ on Fab and 240 $Å^2$ on peptide) (Figure 5d).

Most of the BSA contributions from heavy chain come from residues ^{10}PNANPNV^{15} in both Fabs 7088 and MS-1805 with the N-terminal junctional peptide (Figure S4A). Similarly, in Fabs 7088 and MS-1805 with $NPNA_3$, the majority of the BSA from the heavy chain is from ^{6}PNANPNA^{12} (Figure S4B), indicating that the minimal epitope PNANPN is necessary for both junctional and major repeat peptides.

Furthermore, the MS-1805 peptide complex exhibited similar Trp-Pro and other aromatic interactions as observed in Fab 7088 with $NPNA_3$ and junctional region peptides, with both complexes engaging in CH/π interactions with germline-encoded ^{H}Trp^{52} and ^{H}Tyr^{58} in CDRH2 (Figure 5e). Interestingly, we noted that ^{L}Phe^{95A} in 7088 and engineered MS-1805 Fab participate in CH/π interactions with proline in the short major repeat and N-terminal junctional epitopes. This interaction is distinct from the other known Fabs that are encoded by the IGHV3-33/IGKV1-5 germline genes (Murugan et al., 2020; Thai et al., 2023).

2.4 | Highly protective mAb Fab 7088 and engineered variant Fab MS-1805 feature an extended CDRL3 compared to other antibodies encoded by the IGHV3-33/1GKV1-5 germlines

Previous studies have shown that antibodies capable of cross-reacting with the NANP repeat peptide are often encoded by IGHV3-33 paired with IGKV1-5 (Thai et al., 2023). Several crystal structures of Fabs derived from the IGHV3-33/IGKV1-5 germline have been determined. To better understand the molecular recognition of antibodies from these specific germlines, we compared crystal structures of MS-1805 with $NPNA_3$ to other antibodies, including Fabs 850, 1210, 2541, and 2243, also in complex with major repeat region peptides (Kucharska et al., 2022; Murugan et al., 2020) (Figure 6).

All of these Fabs exhibit similar conformations of CDRH1, CDRH2, and CDRH3, suggesting conserved interactions with their respective epitopes. However, a key difference was that MS-1805 possesses a CDRL3 of 10 amino acids (CDRL3:10), whereas CDRL3 of other related CSP repeat antibodies encoded by this germline is typically 8 amino acids (CDRL3:8). Interestingly, while a tyrosine at position 94 in CDRL3 of the other Fabs forms CH/π interactions with proline, MS-1805 has phenylalanine at position 95A in CDRL3 that engages in similar CH/π interactions (Figure 6a). To further understand how the extended CDRL3 is accommodated in MS-1805, we superimposed its crystal structure with that of previously characterized Fab 850 with $NPNA_3$ (PDB ID: 7UYM) (Kucharska et al., 2022). In Fab MS-1805, CDRL3 is extended at its tip by Ser and Tyr at positions 93 and 94, and ^{L}Ser^{95} and ^{L}Phe^{95A} now occupy positions corresponding to ^{L}Asn^{93} and ^{L}Tyr^{94} in Fab 850 (Figure 6b). Additionally, CDRL3:8 in Fab 850 has fewer hydrogen-bond interactions with its epitope compared to CDRL3:10 in Fab MS-1805, where ^{L}Ser^{95} and ^{L}Phe^{95A} form additional interactions (Figure 6c). Furthermore, the BSA contributed by CDRL3 in MS-1805 is 189 $Å^2$ on Fab and 248 $Å^2$ on the peptide, substantially higher than the BSA contributed by CDRL3 in Fab 850 (111 $Å^2$ on Fab and 165 $Å^2$ on the peptide) (Figure 6d). Taken together, these results demonstrate that the extended CDRL3 of MS-1805 plays a critical role in the unique binding profile, providing enhanced specificity and interaction density relative to other IGHV3-33/IGKV1-5 antibodies. This structural adaptation may underlie the unique recognition properties of MS-1805 and suggests potential advantages for its application as a therapeutic antibody.

2.5 | Cryo-EM analysis of Fab 224 and 7088 in complex with rsCSP reveals that 7088 is a homotypic antibody, a feature also conserved in the engineered mutants

Previous cryo-electron microscopy (cryo-EM) analysis of several CSP repeat-binding antibodies revealed that many adopt homotypic configurations upon binding to CSP, with Fab-Fab interactions leading to an oligomeric complex of multiple Fab molecules binding to one antigen. (Martin et al., 2023; Oyen et al., 2017).

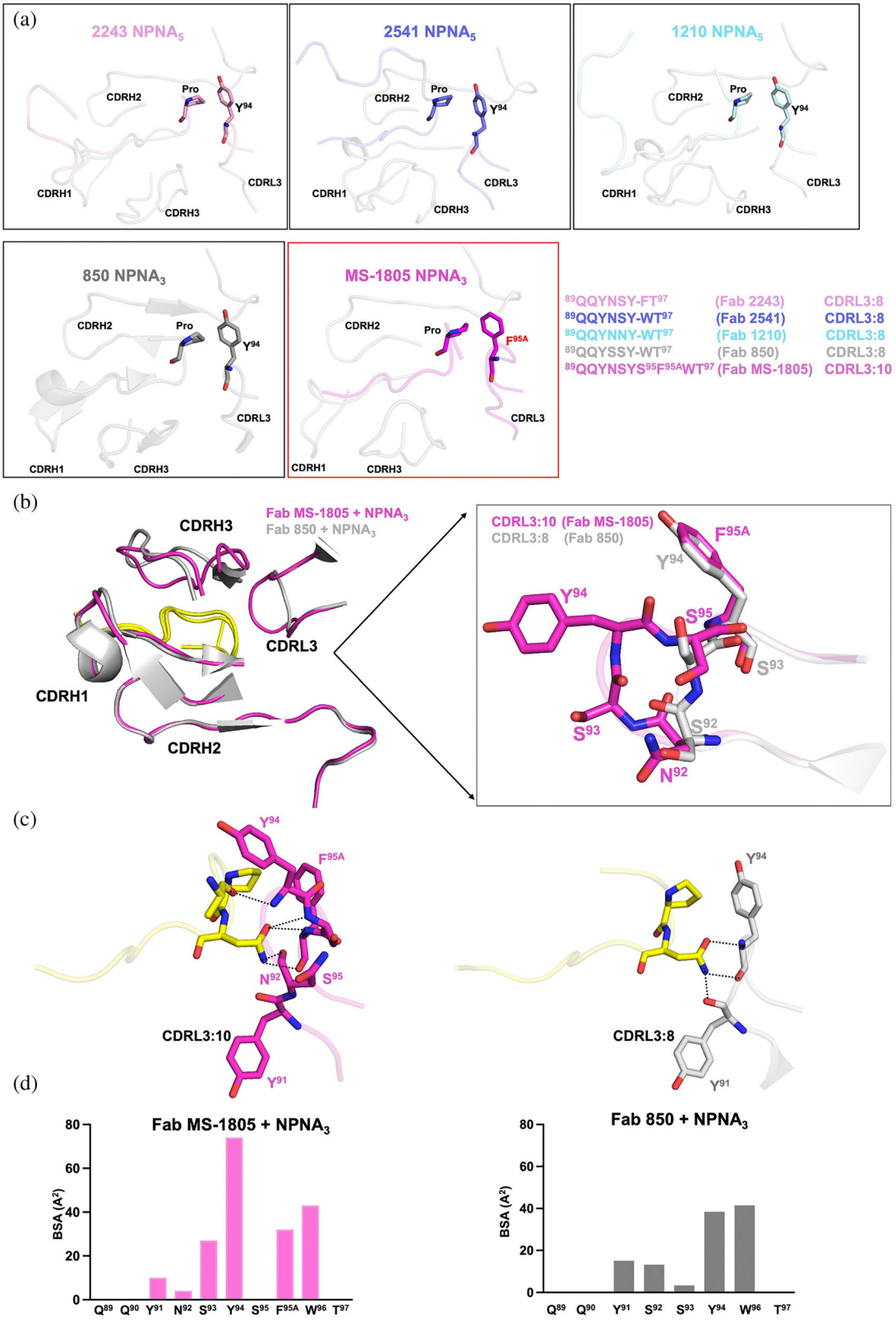

FIGURE 6 Structural comparison of Fabs to CSP encoded by IGHV3-33/IGKV1-5 germline genes. (a) Semi-transparent cartoon representation of Fab MS-1805 (magenta) with other IGHV3-33/IGKV1-5 Fabs 850 (gray), 1210 (cyan), 2541 (slate blue), and 2243 (pink), each complexed with peptides (yellow). CH/π interactions of Phe^{95A} in CDRL3 of Fab MS-1805 and Tyr^{94} in CDRL3 of Fab 850 (PDB ID: 7UYM), Fab 1210 (PDB ID: 6D01), 2541 (PDB ID: 6ULE), and 2243 (PDB ID: 6O23) engaged with proline are shown as sticks and highlighted in their respective colors. (b) Superposition of Fab MS-1805 and Fab 850 with $NPNA_3$, highlighting their CDRL3 conformations. (c) Hydrogen-bond interactions (black dashes) between Fab MS-1805 (magenta) and Fab 850 (gray) with the short major repeat peptide (yellow). (d) Bar plot shows the individual residues of CDRL3 that contribute to the buried surface area of Fab MS-1805 (colored in magenta) and Fab 850 (colored in gray). Crystal structure of Fab 850 complexed with $NPNA_3$ was obtained from a previous study (PDB ID: 7UYM).

We, therefore, used cryo-EM to first assess whether Fabs 224 and 7088 formed homotypic interactions and, second, if this state was in any way altered in the engineered counterpart. The cryo-EM analysis of 7088 Fab with a recombinant, truncated CSP (rsCSP) led to a 3.7 Å cryo-EM reconstruction (Figure S5 and Table S4) and revealed that it does indeed adopt a homotypic, right-handed spiral conformation, similar to other homotypic spirals previously reported (Martin et al., 2023). One of the protomers in the cryo-EM Fab-rsCSP complex is equivalent to the x-ray structure reported above (Figure S6), and we therefore focus on the homotypic interactions observed in cryo-EM. For clarity, considering the repetitive nature of homotypic spirals and of the CSP repeat-rich region, the residues described are referred to according to their Kabat numbering (Fabs) and position in the core CSP epitope (^{1}NPNANP-NANPNA^{12}), regardless of the position of an individual Fab or epitope in the spiral. In the 7088 spiral, the CDRH3 region of the Fab molecule binds simultaneously with the rsCSP core epitope and neighboring antibody, in what we refer to as Interface 1 (Figure 7a). The ^{H}Arg^{96} forms a salt-bridge with the neighboring CDRH2 ^{H}Asp^{61}, while ^{H}Phe^{97} is coordinated in a π-stacking interaction involving Pro^{10} on CSP and the neighboring Fab heavy chain ^{H}Tyr^{58} and light chain ^{L}Phe^{95A} (Figure 7a, left). These interactions enable the nearby light chain ^{L}Tyr^{94} to be involved in van der Waals interactions with CSP Asn^{5} and Asn^{9}, thereby acting as a glue between two adjacent epitopes as the spiral bends (Figure 7a, right). The rest of the interface is stabilized by hydrogen bonds (^{H}Thr^{31}-^{H}Tyr^{58}) between the heavy chains of neighboring Fabs. Finally, as the spirals wrap around to form a full turn of the helical structure, the Fabs in one turn of the spiral form a dense network of salt-bridges and hydrogen bonds with the Fabs stacked above or below in the long-range spiral configuration. The main residues involved in this Interface 2 include ^{H}Arg^{19}, ^{H}Ile^{68}, ^{H}Ser^{70}, ^{H}Asp^{72}, and ^{H}His^{74} on the heavy chain, with the ^{L}Ser^{65}, ^{L}Glu^{70}, ^{L}Ser^{67}, ^{L}Ser^{31}, and ^{L}Ser^{30} on the adjacent light chain (Figure 7b). In all, the CDRH3-related interface alone accounts for 255 Å^2 of buried surface area, and the second, top-bottom interface is 228 Å^2 (Figure 7c).

We then analyzed the engineered MS-1805 by cryo-EM (Figure S6) and observed that it also adopts a homotypic conformation, similar to 7088, with an RMSD of 1.14 Å for the whole complex (RMSD of 0.79 Å for rsCSP alone) (Figure S7). Some of the mutations in this engineered construct are of particular interest as they are near the homotypic interfaces and participate in stabilizing the spiral. At the interface between two juxtaposed Fabs, ^{H}Thr^{68} is now able to form a hydrogen bond with the nearby ^{L}Glu^{70} from the adjacent light chain, while ^{H}Tyr^{79} stabilizes ^{H}Arg^{19} as it interacts with the ^{L}Ser^{65} in the FR3 region of the light chain (Figure 7d). Meanwhile, at the interface between two side-by-side Fabs, ^{H}Thr^{28} is now in prime position to hydrogen bond with the neighboring ^{H}Gln^{56}. Therefore, while the mutations in the engineered MS-1805 did not have a direct role in CSP binding, half of them contribute to the homotypic interfaces for the MS-1805 antibody.

We also attempted to image Fab 224 by cryo-EM; however, this antibody did not adopt any homotypic state and only disordered 2D classes of Fab were observable with enough flexibility between the Fab molecules to hinder attempts at 3D reconstruction (Figure S8); the engineered mutant MAM01 did not adopt a homotypic conformation either, with 2D classes displaying even more flexibility, meaning that, in this case as well, the mutations to improve the antibody did not have an impact on the homotypic state observed for this particular antibody (Figure S8).

In conclusion, the selection process undertaken during the generation of MAM01 led to two candidate antibodies that, despite similar efficacy, differed substantially in the quaternary structures they could adopt, as 7088 adopts a spiral, homotypic state, while 224 does not show any homotypic conformation. We demonstrated that the mutations introduced during the engineering process did not alter the homotypic status of any of them, while potentially maintaining or promoting the spiral conformation of 7088/ MS-1805 by enhancing the contacts at the different homotypic interfaces.

2.6 | The unliganded structure of Fab MAM01 and MS-1805 shows small conformational changes in their CDR side chains upon peptide binding

We determined unliganded crystal structures of MAM01 and MS-1805 at resolutions of 2.08 Å and 1.77 Å, respectively, to investigate any conformational changes upon binding to CSP peptides (Table S5). We superimposed the unliganded structure of MAM01 with its peptide-bound forms. We observed changes in the orientation of some side chains in the CDRs in the Fab MAM01 unliganded structure compared to the liganded structures. The aromatic side chains of ^{H}Tyr^{53} in CDRH2, ^{H}Tyr^{100E} and ^{H}Tyr^{100F} in CDRH3, and ^{L}Trp^{96} in CDRL3 of MAM01 showed some movement, mainly in their rotamers, when bound to the peptides (Figure S9A). Similar side-chain reorientations were seen in unliganded Fab 224 when compared to its NPNA$_3$-bound structure, with notable movements in ^{H}Tyr^{100E}, ^{H}Tyr^{100F} in CDRH3, ^{L}Trp^{96} in CDRL3, and ^{H}Arg^{52} in CDRH2 (Figure S9B). In the unliganded MS-1805 structure, slight shifts were observed for the tip of CDRH3 residues 98-100C that include peptide contact residues ^{H}Ser^{98}, ^{H}Pro^{100A}, and ^{H}Gly^{100C} (Figure S9C).

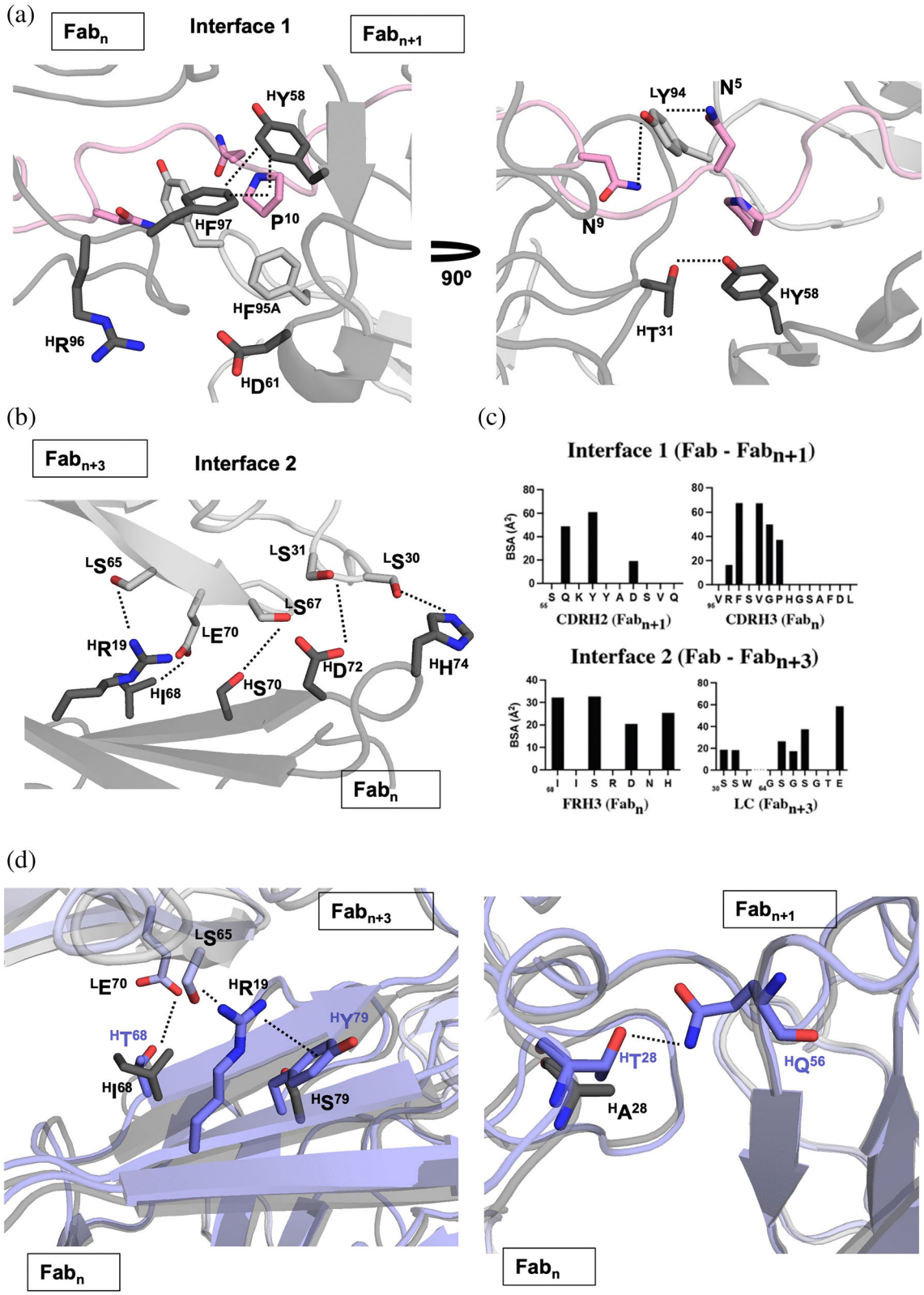

FIGURE 7 Cryo-EM analysis of Fab-7088 and MS-1805 in complex with rsCSP. (a) Homotypic interface 1 between adjacent Fab molecules (Fab$_n$, Fab$_{n+1}$) on the 7088 spiral, focusing on the interaction around CDRH3. The heavy chain (dark gray), light chain (light gray), and CSP (pink) are represented as cartoons, with noteworthy residues highlighted as sticks, with heteroatoms colored. (b) Homotypic interface 2 between Fab molecules stacked above one another after one turn of the spiral (Fab$_n$, Fab$_{n+3}$). Color as in A. (c) Buried surface area of most residues involved in Interface 1 and 2, and with a BSA greater than 15 Å^2. (d) Interfaces 1 and 2, overlapping MS-1805 (HC: dark blue, LC: light blue) and 7088 (HC: dark gray, LC: light gray). Residues from MS-1805 (blue) and Fab-7088 (gray) are shown as sticks, along with the residues they interact with in MS-1805.

3 | DISCUSSION

This study focused on the structural analysis of highly protective and engineered monoclonal antibodies MAM01 and MS-1805, which are derived from different heavy and light chain germline genes and bind to different regions of CSP-derived peptides. MAM01 has been and is currently in clinical trials (US, Uganda) and is being evaluated for use as a seasonal prophylactic treatment for malaria, particularly in pediatric populations in malaria-endemic regions. Recent clinical data demonstrate that MAM01 is safe and well-tolerated in malaria-naive adults and, at higher doses, can prevent detectable infection following controlled human malaria infection (Lyke et al., 2026). These results provide strong proof of concept that passive immunization with an anti-CSP monoclonal antibody can confer protection against malaria and underscore the potential of MAM01 as a viable prophylactic intervention. Together, these findings support continued clinical development, including optimization of dosing strategies and further evaluation in malaria-endemic populations.

Our structural and binding analyses offer a mechanistic framework for these clinical observations. We observed that MAM01 Fab binds to several epitopes, including the junctional region, minor repeat region, and major repeat region, with similar secondary type I β-turn structural conformations. Comparing the engineered Fab MAM01 with Fab 224 in their respective complexes with an $NPNA_3$ repeat peptide revealed that the mutations in the framework region of the MAM01 variable domains do not cause any conformational changes or disrupt interactions with its epitope. Other highly protective engineered mAbs L9LS and CIS43LS, which bind specifically to minor (NVDP) and junctional (NPDP) regions, respectively, are also in clinical trials (Nekkab & Penny, 2022). It will be interesting to investigate and compare the in vivo study of the engineered antibodies MAM01, L9LS, and CIS43LS, which would provide valuable insights into their efficacy against malaria.

Another monoclonal antibody, 7088, is derived from a predominant lineage, IGHV3-33/IGKV1-5, which is elicited by RTS,S vaccinees and exhibits a trend similar to MAM01, also showing superior protection against malaria compared to 317 in a parasitemia challenge model (Williams et al., 2024). This mAb was engineered, renamed MS-1805, and initially selected as an alternative candidate to MAM01; however, no clinical trials have been initiated. Crystal structures of Fab 7088 and engineered MS-1805 in complex with N-terminal junctional peptide and short major repeat ($NPNA_3$) reveal almost identical conformations and similar hydrogen bonding interactions with their epitopes. The majority of crystal structures to the NPNA repeat region are encoded by the germline lineage IGHV3-33 (Pholcharee et al., 2021). Fab MS-1805 has similar germline-encoded $^{H}Trp^{52}$ and $^{H}Tyr^{58}$ CH/π interactions with proline. Interestingly, we observed that CDRL3 of Fab MS-1805 is longer than other known antibodies to CSP NPNA repeats encoded by the same light chain lineage. The longer CDRL3 of MS-1805 showed an increase in the buried surface area and interactions with its epitopes compared to other antibodies encoded by the same germline gene. It will be interesting to determine whether the longer CDRL3 affects any functional properties in a biological or therapeutic setting. Furthermore, our cryo-EM analysis revealed that Fab 7088 and its engineered variant MS-1805 are able to adopt a higher-order spiral structure characteristic of affinity-matured Fab-Fab homotypic interactions. Several of the residues mutated in the engineered variant of the Fab are found at the homotypic interfaces and directly interact with neighboring residues, without destabilizing the spiral. These Fab-Fab interactions are presented as structural features shared with other anti-CSP antibodies, rather than as evidence that these interactions directly contribute to parasite neutralization or enhanced protection. On the other hand, neither Fab 224 nor the MAM01 engineered construct showed any indication of homotypic contacts. These antibodies do not share the same parental lineage, and further structural studies will be needed to better characterize which antibody lineages are able to form homotypic interactions or which ones are not.

Although both 224 (MAM01) and 7088 (MS-1805) monoclonal antibodies were isolated from B cells of protected RTS,S vaccinees, they recognize epitopes in addition to NPNA repeats, including junctional and minor repeat regions, which are not present in RTS,S. From our structural analysis, we observed that the majority of the BSA contribution is mediated by the PNANPN sequence that is present in the junctional, minor, and major repeat regions. Although these antibodies were likely affinity-matured against the major repeat, they nevertheless exhibit promiscuous binding to PNANPN in the context of junctional and minor repeat regions. Structural analysis of MAM01 and MS-1805 showed that these cross-reactive human mAbs recognize distinct epitopes of *P. falciparum* circumsporozoite protein, each epitope adopting a specific secondary structural motif, corresponding either to type I β-turn or Asn pseudo 3_{10} turn conformations.

The NPDP junctional and NVDP minor repeat motif of PfCSP, which is targeted by both protective mAbs, represents a neutralizing epitope that is not present in the RTS,S vaccine. These findings confirm that incorporating these epitopes could enhance the effectiveness of future malaria vaccines (Cockburn & Seder, 2018; Flores-Garcia et al., 2021; Langowski et al., 2022; Murugan et al., 2020; Wang et al., 2020). Overall, these engineered antibodies, MAM01 and MS-1805, are a promising advance in malaria prevention

due to their mechanism of action, successful manufacture, and long-acting formulation.

4 | MATERIALS AND METHODS

4.1 | Protein expression and purification

Antibody sequences of heavy chain and light chain variable regions were obtained from Atreca and are available in (Williams et al., 2024). The Fab genes of MAM01, 7088, and MS-1805 were codon optimized for mammalian expression and cloned into the expression vector PHCMV3 by GenScript. The Fabs were transiently expressed in ExpiCHO cells according to the manufacturer's recommended protocol. Briefly, ExpiCHO cells were maintained in ExpiCHO Expression Medium at 37°C with 8% CO_2 under constant shaking at 125 rpm. Cells were transfected at a density of approximately 6×10^6 cells/mL using plasmids encoding the heavy and light-chain constructs together with the ExpiFectamine CHO transfection reagent. Following transfection, enhancer feeds were added according to the standard ExpiCHO expression protocol, and cultures were maintained for 10–12 days to allow optimal protein expression. Culture supernatants were harvested by centrifugation at 4000 × *g* for 30 min and further clarified by filtration through a 0.22 μm membrane filter. The clarified supernatant was loaded onto a HiTrap Protein G HP affinity column (GE Healthcare) pre-equilibrated with phosphate-buffered saline (PBS). After extensive washing to remove non-specifically bound proteins, bound Fabs were eluted using 0.1 M glycine-HCl buffer (pH 3.0) and immediately neutralized with 1 M Tris–HCl (pH 8.0). Eluted fractions containing Fab proteins were pooled and concentrated using centrifugal ultrafiltration devices with an appropriate molecular weight cutoff. The concentrated samples were further purified by size exclusion chromatography using a Superdex 200 16/90 column (GE Healthcare) equilibrated in 1× Tris-buffered saline (TBS; 50 mM Tris–HCl, pH 7.8, 140 mM NaCl).

4.2 | Bio-layer interferometry

Binding kinetics of Fabs 224, MAM01, 7088, and MS-1805 to PfCSP epitopes were measured by biolayer interferometry (BLI) using an Octet Red instrument (Pall ForteBio). Biotinylated peptides (Innopep Inc.) were diluted to 10 μg/mL in kinetics buffer (1× PBS, 0.01% BSA, 0.002% Tween 20) and immobilized on streptavidin biosensors. Biotinylated rsCSP was similarly loaded onto streptavidin biosensors (Pall ForteBio, cat. no. 18-5019) at 10 μg/mL. Sensors were equilibrated in kinetics buffer and then exposed to Fab analytes at concentrations of 200, 100, 50, 25, and 12.5 nM. The assay consisted of baseline (60 s), antigen loading (60 s), baseline (60 s), association (300 s), and dissociation (300 s) steps. Reference sensors incubated in buffer alone were used for background subtraction to account for non-specific binding. Data were analyzed using Octet data analysis software (v12.2) and fitted with a 1:1 binding model to determine kinetic parameters. All BLI measurements were conducted in at least two independent experiments, and the results were reproducible between experiments. Representative sensorgrams are shown, and fits were evaluated based on R^2 values.

4.3 | Fab-peptide complexes

All the CSP-derived peptides had protection of their amine and carboxyl groups at the N-term and C-term with acetyl and amine groups: Ac-KQPADGNPDPNANPNV-NH_2 (N-terminal junctional region peptide), Ac-NPDP NANPNVDPNANP-NH_2 (Junctional region peptide), Ac-NVDPNANPNVDPNANPNVDP-NH_2 (Minor repeat region peptide), Ac-NPNANPNANPNA-NH_2 (Short major repeat region peptide), and Ac-NANPNANPNANPNANP-NANPNANP-NH_2 (Long major repeat region peptide). Peptides were ordered from Innopep Inc. with high (98%) purity. MAM01Fab was concentrated to 11 mg/mL in 1X TBS using 10 K Amicon ultra centrifugal units and further mixed with junctional, minor, and major repeat peptides in a 1:5 molar ratio of Fab to peptide. Similarly, 7088 Fab and MS-1805 Fab were concentrated to 10 mg/mL in 1X TBS and mixed with N-terminal junctional and short major repeat peptides in a 1:5 molar ratio of Fab to peptide and stored at 4°C overnight.

4.4 | Crystallization

All crystal screening was performed using our high-throughput robotic CrystalMation system (Rigaku) at TSRI. Crystals were grown using the sitting drop vapor diffusion method with a reservoir solution of 35 μL, with each drop consisting of 0.1 μL of protein and 0.1 μL precipitant. Crystals for Fab MAM01 complexed with the junctional peptide were grown in 0.085 M Tris, pH 8.5, 0.17 M sodium acetate, 15% (v/v) glycerol, and 25.5% (w/v) polyethylene glycol 4000. Fab MAM01 with the minor repeat peptide was grown in 0.2 M potassium acetate, pH 7.8, and 20% (w/v) polyethylene glycol 3350 and cryoprotected in 10% ethylene glycol. Fab MAM01-$NPNA_3$ cocrystals were grown in 0.1 M Bicine, pH 9.0, and 65% (v/v) 2-methyl-2,4-pentanediol. Crystals of the Fab MAM01-$NANP_6$ complex were grown in 0.04 M potassium dihydrogen phosphate, 20% (v/v) glycerol, and 16% (w/v) polyethylene glycol 8000. Crystals for MAM01-apo were grown in 0.1 M MES pH 6.0 and 30% (w/v) polyethylene glycol 6000 and

cryoprotected in 10% PEG 200. Crystals for Fab 224-apo were grown in 0.17 M ammonium sulfate, 15% (v/v) glycerol, 25.5% (w/v) PEG4000. All crystals for Fab MAM01 and Fab 224 complexed with or without their peptides appeared within 7 days at 293 K.

Crystals for 7088 Fab with junctional region peptide were grown in 0.1 M Tris, pH 8.0, 1 M lithium chloride, and 10% (w/v) polyethylene glycol 6000 and cryoprotected in 15% ethylene glycol. Crystals for 7088-$NPNA_3$ complex were grown in 0.2 M sodium chloride and 20% (w/v) polyethylene glycol 3350 and cryoprotected in 15% ethylene glycol. Co-crystals of MS-1805 Fab with junctional peptide were grown in 0.1 M sodium citrate, 20% (v/v) 2-propanol, and 20% (w/v) polyethylene glycol 4000, and Fab 1805 with $NPNA_3$ were grown in 0.2 M zinc acetate and 20% (w/v) polyethylene glycol 3350; both sets of crystals were cryoprotected in 10% ethylene glycol. Crystals for Fab MS-1805 apo were grown in 0.095 M sodium citrate pH 5.6, 19% (v/v) 2-propanol, 5% glycerol, and 19% (w/v) polyethylene glycol 4000. All crystals for Fab 7088 and 1805 with or without peptides appeared within 14–21 days at 293 K.

4.5 | X-ray data collection and structure determination

X-ray diffraction data for MAM01 Fabs with or without peptides were collected at Stanford Synchrotron Radiation Lightsource (SSRL) beamline BL12-1 (Tables S2, S5). For Fabs 7088 and MS-1805 with or without peptides, x-ray diffraction data were collected at National Synchrotron Light Source II beamline 17-ID-1 (highly automated macromolecular crystallography—NSLS-II AMX) (Tables S3, S5). X-ray diffraction data for Fab 224 apo were collected at National Synchrotron Light Source II beamline 17-ID-2 (Frontier Micro Focusing Macromolecular Crystallography—NSLS-II FMX). All diffraction data were processed and scaled using the HKL-2000 package (Otwinowski & Minor, 1997). The structures of MAM01 Fab were solved by molecular replacement with PHASER (McCoy et al., 2007) using Fab 224 (PDB ID: 6WFY) as a search model. The structures of 7088 Fab were solved by molecular replacement with PHASER using a homology model generated with SWISS-MODEL (Bienert et al., 2017; Guex et al., 2009), and subsequent MS-1805 Fab structures were solved using Fab 7088 as the search model. All Fab structures were refined using phenix.refine, combining with model building cycles in Coot (Adams et al., 2010; Emsley et al., 2010). The peptides were manually fitted into the Fo-Fc electron density maps with multiple rounds of refinement in phenix.refine (Adams et al., 2010). The residue numbering of the Fabs follows Kabat nomenclature, and structure validation was done with MolProbity (Williams et al., 2018). Buried surface areas were calculated using the program MS (Connolly, 1993), and hydrogen bonds were assessed using the program HBPLUS for structure analysis (McDonald & Thornton, 1994).

4.6 | Cryo-EM sample preparation and data collection

For each complex, 166 μg of Fab was mixed with 10 μg of rsCSP. After overnight incubation at 4°C, complexes were purified by size-exclusion chromatography on a Superdex 200 10/300 column (GE Healthcare). Grids (Quantifoil 1.2/1.3300-mesh copper grid) were blotted for 5 s after a 10 s wait time in a Vitrobot Mark IV (ThermoFisher) at 4°C and 100% humidity. Movies were collected on a Glacios microscope (200 keV) equipped with a Falcon IV detector (ThermoFisher) for Fab 224, 7088, or a Glacios 2 microscope (200 keV) equipped with a Falcon 4i detector (ThermoFisher) for MAM-01 and MS-1805. Nominal magnification on the Glacios was 190,000× with a pixel size of 0.725 Å, and nominal magnification on the Glacios 2 was 190,000× with a pixel size of 0.718 Å. Data were collected at an average dose rate of 60 $e^-/Å^2$ with a defocus between −0.6 and −1.6 μm.

4.7 | Cryo-EM data processing and model building

CryoSPARC (Punjani et al., 2017) and CryoSPARC Live were used for data processing. After preprocessing with Patch Motion Correction and CTF estimation by cryoSPARC Live, movies with a CTF fit higher than 10 Å were rejected from further processing. An initial batch of 17k particles was picked with Blob Picker (minimal diameter 140 Å) to select four 2D classes used as templates for Template Picking on all micrographs for Fab 7088, for a total of 650k particles. Subsequently, only the Blob picker was used for MS-1805 particle picking, for a total of 600k particles. After 2D and 3D classifications, a final set of 73,108 particles (Fab 7088) or 112,207 particles (Fab MS-1805) was selected for high-resolution ab-initio model building, based on recent published pipelines (Kim et al., 2025). Homogeneous Reconstruction was followed by Local Refinement with a mask focusing on the variable domains of the Fab molecules. We used ModelAngelo (Jamali et al., 2024) to build the initial antibody fragments into the density, after which iterations of model building were performed in Coot (Emsley et al., 2010), refined using Phenix (Adams et al., 2010), and validated with MolProbity (Williams et al., 2018) (Table S4).

AUTHOR CONTRIBUTIONS

Randal R. Ketchem: Resources. **Daniel E. Emerling:** Resources; writing – review and editing. **Gonzalo E. González-Páez:** Methodology; data curation. **Wen-Hsin Lee:** Methodology; data curation. **Fabien Cannac:** Methodology; data curation; visualization; formal analysis; writing – review and editing; investigation; writing – original draft. **Re'em Moskovitz:** Formal analysis; writing – review and editing. **Monika Jain:** Conceptualization; methodology; investigation; validation; formal analysis; data curation; writing – original draft; visualization; writing – review and editing. **Andrew B. Ward:** Funding acquisition; supervision; resources; conceptualization; validation; writing – review and editing. **Ian A. Wilson:** Supervision; writing – review and editing; funding acquisition; validation; visualization; resources; project administration; writing – original draft. **Katherine L. Williams:** Resources; writing – review and editing. **Sashank Agrawal:** Validation; formal analysis; visualization; investigation; data curation; writing – review and editing.

ACKNOWLEDGMENTS

We thank Atreca, Inc. for providing the antibody sequences of heavy chain and light chain variable regions of the engineered Fabs MAM01 and MS-1805, as also reported in Williams et al., 2024. This work was supported and funded by the Gates Foundation (INV-004923 and INV-056202) under a collaborative agreement with The Scripps Research Institute. The conclusions and opinions expressed in this work are those of the author(s) alone and shall not be attributed to the Foundation. Under the grant conditions of the Foundation, a Creative Commons Attribution 4.0 License will be assigned to the Author Accepted Manuscript version that might arise from this submission. We also acknowledge Henry Tien for helping with the automated robotic crystal screening at The Scripps Research Institute, Jacqueline Kirchner of the Gates Foundation for support and helpful comments, and Jared Silverman of the Gates Medical Research Institute for reading the manuscript and providing useful comments. Use of the Stanford Synchrotron Radiation Lightsource, SLAC National Accelerator Laboratory, is supported by the U.S. Department of Energy, Office of Science, Office of Basic Energy Sciences under Contract No. DE-AC02-76SF00515. The SSRL Structural Molecular Biology Program is supported by the DOE Office of Biological and Environmental Research, and by the National Institutes of Health, National Institute of General Medical Sciences (P30GM133894). The contents of this publication are solely the responsibility of the authors and do not necessarily represent the official views of NIGMS or NIH. This research used resources beamlines FMX and AMX of the National Synchrotron Light Source II, a U.S. Department of Energy (DOE) Office of Science User Facility operated for the DOE Office of Science by Brookhaven National Laboratory under Contract No. DE-SC0012704.

CONFLICT OF INTEREST STATEMENT

M.J., S.A., F.C., G.G.-P, W-H.L., R.M., A.B.W., and I.A.W. have declared that no competing interests exist. K.L.W. and R.R.K. have worked for Atreca, Inc. and Just-Evotec Biologics, respectively. D.E.E. is a consultant for Atreca, Inc.

DATA AVAILABILITY STATEMENT

The authors declare that all the data supporting the findings of this study are available within the manuscript and supplementary information files. The structure factors and coordinates of MAM01 bound to junctional, minor, short major repeat, and long major repeat regions have been deposited in the Protein Data Bank (PDB) with accession codes 9NL1, 9NZF, 9NL0, and 9NKZ, respectively. Similarly, the structure factors and coordinates of 7088 bound to the N-terminal junctional and short minor repeat regions and MS-1805 bound to the N-terminal junctional and short minor repeat regions have been deposited with PDB accession codes 9DSU, 9DSS, 9DST, 9DSR, respectively. The structure factors and coordinates of 224, MAM01and MS-1805 in apo form have been deposited with PDB accession codes 9NOB, 9NKY and 9NOA. respectively. Cryo-EM structures and corresponding density maps generated in this study for 7088-rsCSP have been deposited in the Protein Data Bank (PDB) and Electron Microscopy Data Bank (EMDB), respectively, under accession codes 12HK and EMD-76437. Similarly, Cryo-EM structures and corresponding density maps generated in this study for MS-1805-rsCSP have been deposited in the PDB and EMDB, respectively, under accession codes 12HL and EMD-76438.

ORCID

Monika Jain https://orcid.org/0000-0001-8700-4562
Sashank Agrawal https://orcid.org/0000-0001-8549-9602
Randal R. Ketchem https://orcid.org/0000-0002-7821-2682
Daniel E. Emerling https://orcid.org/0000-0002-8754-9201
Ian A. Wilson https://orcid.org/0000-0002-6469-2419

REFERENCES

Adams PD, Afonine V, Bunkóczi G, Chen VB, Davis IW, Echols N. PHENIX: a comprehensive Python-based system for macromolecular structure solution. Acta Crystallogr D Biol Crystallogr. 2010;66(Pt 2):213–21.

Bienert S, Waterhouse A, de Beer TA, Tauriello G, Studer G, Bordoli L, et al. The SWISS-MODEL repository-new features and functionality. Nucleic Acids Res. 2017;45(D1):D313–9.

Cockburn IA, Seder RA. Malaria prevention: from immunological concepts to effective vaccines and protective antibodies. Nat Immunol. 2018;19:1199–211.

Connolly ML. The molecular surface package. J Mol Graph. 1993;11: 139–41.

Datoo MS, Dicko A, Tinto H, Ouedraogo JB, Hamaluba M, Olotu A, et al. Safety and efficacy of malaria vaccine candidate R21/-matrix-M in African children: a multicentre, double-blind, randomised, phase 3 trial. Lancet. 2024;403:533–44.

Ducancel F, Muller BH. Molecular engineering of antibodies for therapeutic and diagnostic purposes. MAbs. 2012;4:445–57.

Emsley P, Lohkamp B, Scott WG, Cowtan K. Features and development of coot. Acta Crystallogr D Biol Crystallogr. 2010;66(Pt 4): 486–501.

Flores-Garcia Y, Wang LT, Park M, Asady B, Idris AH, Kisalu NK, et al. The *P. falciparum* CSP repeat region contains three distinct epitopes required for protection by antibodies in vivo. PLoS Pathog. 2021;17:e1010042.

Gaudinski MR, Berkowitz NM, Idris AH, Coates EE, Holman LA, Mendoza F, et al. A monoclonal antibody for malaria prevention. N Engl J Med. 2021;385:803–14.

Guex N, Peitsch MC, Schwede T. Automated comparative protein structure modeling with SWISS-MODEL and Swiss-PdbViewer: a historical perspective. Electrophoresis. 2009;30(Suppl 1): S162–73.

Imkeller K, Scally SW, Bosch A, Marti GP, Costa G, Triller G, et al. Antihomotypic affinity maturation improves human B cell responses against a repetitive epitope. Science. 2018;360: 1358–62.

Jamali K, Kall L, Zhang R, Brown A, Kimanius D, Scheres SHW. Automated model building and protein identification in cryo-EM maps. Nature. 2024;628:450–7.

Kayentao K, Ongoiba A, Preston AC, Healy SA, Doumbo S, Doumtabe D, et al. Safety and efficacy of a monoclonal antibody against malaria in Mali. N Engl J Med. 2022;387:1833–42.

Kayentao K, Ongoiba A, Preston AC, Healy SA, Hu Z, Skinner J, et al. Subcutaneous administration of a monoclonal antibody to prevent malaria. N Engl J Med. 2024;390:1549–59.

Kerwin BA, Bennett C, Brodsky Y, Clark R, Floyd JA, Gillespie A, et al. Framework mutations of the 10-1074 bnAb increase conformational stability, manufacturability, and stability while preserving full neutralization activity. J Pharm Sci. 2020;109: 233–46.

Kim K, Li H, Clarke OB. High-resolution ab initio reconstruction enables cryo-EM structure determination of small particles. bioRxiv. 2025 2025.2009.2008.674935.

Kisalu NK, Pereira LD, Ernste K, Flores-Garcia Y, Idris AH, Asokan M, et al. Enhancing durability of CIS43 monoclonal antibody by Fc mutation or AAV delivery for malaria prevention. JCI Insight. 2021;6:e143858.

Kucharska I, Binter S, Murugan R, Scally SW, Ludwig J, Prieto K, et al. High-density binding to *Plasmodium falciparum* circumsporozoite protein repeats by inhibitory antibody elicited in mouse with human immunoglobulin repertoire. PLoS Pathog. 2022;18:e1010999.

Langowski MD, Khan FA, Savransky S, Brown DR, Balasubramaniyam A, Harrison WB, et al. Restricted valency (NPNA)(n) repeats and junctional epitope-based circumsporozoite protein vaccines against *Plasmodium falciparum*. NPJ Vaccines. 2022;7:13.

Livingstone MC, Bitzer AA, Giri A, Luo K, Sankhala RS, Choe M, et al. In vitro and in vivo inhibition of malaria parasite infection by monoclonal antibodies against *Plasmodium falciparum* circumsporozoite protein (CSP). Sci Rep. 2021;11:5318.

Lyke KE, Berry AA, Laurens MB, Winkler J, Joshi S, Koudjra AR, et al. Human monoclonal antibody MAM01 for protection against malaria in adults in the USA: a first-in-human, phase 1, dose-escalation, double-blind, placebo-controlled, adaptive trial. Lancet Infect Dis. 2026;26:170–81.

Martin GM, Torres JL, Pholcharee T, Oyen D, Flores-Garcia Y, Gibson G, et al. Affinity-matured homotypic interactions induce spectrum of PfCSP structures that influence protection from malaria infection. Nat Commun. 2023;14:4546.

McCoy AJ, Grosse-Kunstleve RW, Adams PD, Winn MD, Storoni LC, Read RJ. Phaser crystallographic software. J Appl Cryst. 2007; 40(Pt 4):658–74.

McDonald IK, Thornton JM. Satisfying hydrogen bonding potential in proteins. J Mol Biol. 1994;238:777–93.

Miura K, Flores-Garcia Y, Long CA, Zavala F. Vaccines and monoclonal antibodies: new tools for malaria control. Clin Microbiol Rev. 2024;37:e0007123.

Murugan R, Scally SW, Costa G, Mustafa G, Thai E, Decker T, et al. Evolution of protective human antibodies against *Plasmodium falciparum* circumsporozoite protein repeat motifs. Nat Med. 2020;26:1135–45.

Nekkab N, Penny MA. Accelerated development of malaria monoclonal antibodies. Cell Rep Med. 2022;3:e100786.

Otwinowski Z, Minor W. [20] processing of X-ray diffraction data collected in oscillation mode. Methods Enzymol. 1997;276:307–26.

Oyen D, Torres JL, Wille-Reece U, Ockenhouse CF, Emerling D, Glanville J, et al. Structural basis for antibody recognition of the NANP repeats in *Plasmodium falciparum* circumsporozoite protein. Proc Natl Acad Sci USA. 2017;114:E10438–45.

Pholcharee T, Oyen D, Flores-Garcia Y, Gonzalez-Paez G, Han Z, Williams KL, et al. Structural and biophysical correlation of anti-NANP antibodies with in vivo protection against *P. falciparum*. Nat Commun. 2021;12:1063.

Punjani A, Rubinstein JL, Fleet DJ, Brubaker MA. cryoSPARC: algorithms for rapid unsupervised cryo-EM structure determination. Nat Methods. 2017;14:290–6.

Regules JA, Cicatelli SB, Bennett JW, Paolino KM, Twomey PS, Moon JE, et al. Fractional third and fourth dose of RTS,S/AS01 malaria candidate vaccine: a phase 2a controlled human malaria parasite infection and immunogenicity study. J Infect Dis. 2016; 214:762–71.

Suh PF, Elanga-Ndille E, Tchouakui M, Sandeu MM, Tagne D, Wondji C, et al. Impact of insecticide resistance on malaria vector competence: a literature review. Malar J. 2023;22:19.

Thai E, Murugan R, Binter S, Burn Aschner C, Prieto K, Kassardjian A, et al. Molecular determinants of cross-reactivity and potency by VH3-33 antibodies against the *Plasmodium falciparum* circumsporozoite protein. Cell Rep. 2023; 42:113330.

Thomson MC, Stanberry LR. Climate change and vectorborne diseases. N Engl J Med. 2022;387:1969–78.

Wang LT, Pereira LS, Flores-Garcia Y, O'Connor J, Flynn BJ, Schon A, et al. A potent anti-malarial human monoclonal antibody targets circumsporozoite protein minor repeats and neutralizes sporozoites in the liver. Immunity. 2020;53:733–744.e8.

Williams CJ, Headd JJ, Moriarty NW, Prisant MG, Videau LL, Deis LN, et al. MolProbity: more and better reference data for improved all-atom structure validation. Protein Sci. 2018;27: 293–315.

Williams KL, Guerrero S, Flores-Garcia Y, Kim D, Williamson KS, Siska C, et al. A candidate antibody drug for prevention of malaria. Nat Med. 2024;30:117–29.

World malaria report. Addressing the threat of antimalarial drug resistance. 2025.

Wu RL, Idris AH, Berkowitz NM, Happe M, Gaudinski MR, Buettner C, et al. Low-dose subcutaneous or intravenous monoclonal antibody to prevent malaria. N Engl J Med. 2022;387: 397–407.

Zalevsky J, Chamberlain AK, Horton HM, Karki S, Leung IW, Sproule TJ, et al. Enhanced antibody half-life improves in vivo activity. Nat Biotechnol. 2010;28:157–9.
Zavala F. RTS,S: the first malaria vaccine. J Clin Invest. 2022;132: e156588.

SUPPORTING INFORMATION

Additional supporting information can be found online in the Supporting Information section at the end of this article.

How to cite this article: Jain M, Agrawal S, Cannac F, González-Páez GE, Lee W-H, Moskovitz R, et al. Engineered antibodies preserve structural and functional recognition of *Plasmodium falciparum* circumsporozoite protein. Protein Science. 2026;35(9):e70738. https://doi.org/10.1002/pro.70738